Temperature Prediction and Optimization Model for Night Flushing

Carlos Duarte & Jared Landsman

CE 295: Energy Systems and Control

Friday May 8th, 2015

Table of Contents

Abstract

We have developed a hybrid (First Principles/Data Driven) model to predict the instantaneous air and mass temperatures of a classroom in the La Escuelita Education Center (LEEC), located in Oakland, CA. The building's primary mode of cooling is night flushing: the use of forced ventilation at night with the combination of thermal mass walls and floors, allowing radiant cooling to take place during the day when the building is occupied. We have obtained trends of the airflow, mass temperature, room temperature, and outdoor air temperature from the school's building management system (BMS) for the months of June to November (the cooling season). With the BMS data set and our prediction model, we have developed a control strategy for the ventilation system to minimize energy and maintain comfortable temperatures.

Introduction

Buildings in the U.S. consume about 40% of the primary energy, where a large percentage goes into HVAC and lighting systems of the building [1]. A strategy that has the potential to reduce energy consumption and peak demand is through thermal storage capacity. There are two versions of building thermal capacity, active and passive. Active building thermal capacity refers to thermal energy storage systems that mechanically create and store chilled water or ice for later use. On the other hand, a passive building thermal storage capacity refers to the use of the building's envelope, internal construction, and furniture to help cool the building throughout the day [2]. Simulation exercises have shown to have an energy reduction potential of 0-35% and a demand peak reductions of up to 15% through the use of this strategy [3]. For this project, we will investigate a semi-passive building thermal storage capacity in which ventilation rates are increased throughout the cooler temperatures of the night to precool the building during summer days. This strategy is commonly known as "night flushing" and has the greatest savings potential when the mass of the building is large and night time ambient temperatures are low [2], [4].

This strategy, along with other passive strategies, are becoming more common as Net Zero Energy Buildings (NZEBs) become more prevalent. That being said, not many data sets from buildings that use night flushing currently exist. This provides a unique opportunity to investigate and optimize its performance in the La Escuelita Education Center Building. This education building is 21,470 ft^2 in size with 10 classrooms that use night flushing. The current controls of the building's night flushing strategy are not optimized resulting in a required morning warmup of the building, preventing the temperatures of thermal mass surfaces from getting too low and making occupants feel thermally uncomfortable. Thus, eliminating the morning warmup of the building will reduce the building's energy consumption and yield greater energy savings.

There will be some challenges in optimizing this building's strategy because there are not many systems like this in the field in which we can reference. Design engineers of the building had to set the control strategy with many assumptions. A positive is that there are laboratory studies and simulation studies that have addressed these issues. For example, Kintner-Meyer and Emery (1994), Braun (2003), and Lui and Henze (2005) established cost functions based on the costs of electricity and demand charges to optimize night flushing strategies and active building thermal capacity strategies [2], [4], [5]. A similar approach will be taken when optimizing the number of night flushing hours for this project. In addition, we do not know which parameters are important to build a first principles model. That is, we do not know if ventilation flow rates or occupancy will be important to build a model. Another challenge in creating a first principles model will be how to take into account the thermal mass of the classroom surfaces. Furthermore, the design team has logged various data that can help with the model, but we are unsure of how to incorporate it.

Technical Description

Methodology

System Modeling

Our first modeling objective was to determine the relationship between supply temperature and ventilation rate with indoor air temperature and mass temperature for a classroom using mechanical night flushing. Our second modeling objective was to determine how this relationship can be used to predict instantaneous air temperature and mass temperature.

To achieve our modeling objective, two different models were created and trialed for parameter identification. Model version 1 directly takes air flow and supply temperature into account. Model version 2 estimates the power from the ventilation system using a conditional state function based on ventilation rate. Details of each model can be seen below. A schematic of model 2 can be seen in figure 1.

Table 1: Description of parameters & variables in dynamical equations

Symbol	***Description***	***Units***		***Subscript***	***Description***
T	Temperature	[°F]		z	Zone
R	Thermal Resistance	[°F-hr/BTU]		a	Ambient
C	Thermal Capacitance	[BTU/°F]		w	Wall
V	Ventilation Rate	[ft^3/hr]		f	Floor
s	Ventilation State	[0/1]		v	Supply
ρ	Density	[lb/ft^3]			
c	Specific Heat	[BTU/lb-°F]			
P	Ventilation Power	[BTU]			

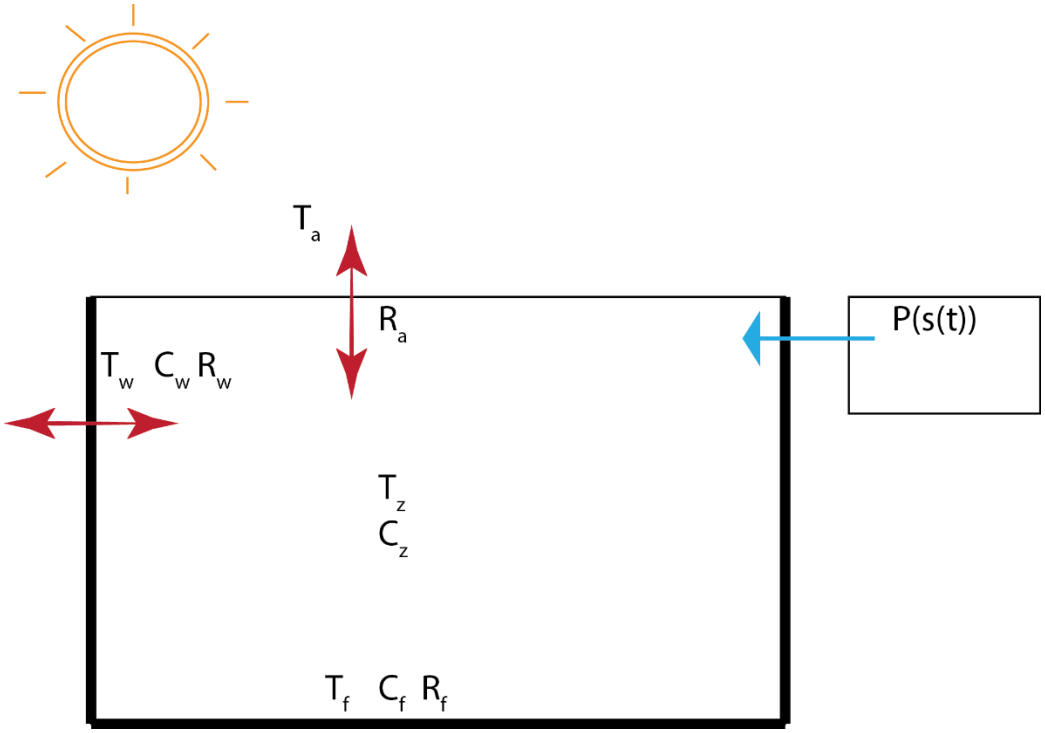

Figure 1: Schematic of model 2

Model Version 1

Controllable Inputs: $V(t)$, $T_V(t)$

Uncontrollable Inputs: $T_A(t)$

Outputs: $T_z(t)$, $T_w(t)$, $T_f(t)$

Parameters: $R_{AZ}, R_{WZ}, R_{FZ}, R_{AW}, C_Z, C_W, C_F, \rho c$

The following are the dynamical equations, state definitions, and input definitions chosen for model 1.

$$C_Z\dot{T}_Z(t) = \frac{1}{R_{AZ}}[T_A(t) - T_Z(t)] + \frac{1}{R_{WZ}}[T_W(t) - T_Z(t)] + \frac{1}{R_{FZ}}[T_F(t) - T_Z(t)] + \rho c V(t)[T_V(t) - T_Z(t)] \quad (1)$$

$$C_W\dot{T}_W(t) = \frac{1}{R_{AW}}[T_A(t) - T_W(t)] + \frac{1}{R_{WZ}}[T_Z(t) - T_W(t)] \quad (2)$$

$$C_F\dot{T}_F(t) = \frac{1}{R_{FZ}}[T_Z(t) - T_F(t)] \quad (3)$$

$$\begin{bmatrix} x_1 \\ x_2 \\ x_3 \end{bmatrix} = \begin{bmatrix} T_z(t) \\ T_w(t) \\ T_f(t) \end{bmatrix} \quad (4)$$

$$\begin{bmatrix} u_1 \\ u_2 \\ u_3 \end{bmatrix} = \begin{bmatrix} T_A(t) \\ V(t) \\ T_V(t) \end{bmatrix} \quad (5)$$

Because equation 1 is non-linear in the inputs & states (4th term), we had to linearize around equilibrium. We chose the first points in our data set as equilibrium points for simplicity. These points were $T_z = 69.5°F$, $T_W = 68.9°F$, $T_F = 67.0°F$, $T_A = 74.0°F$, $V = 0\ cfm$, and $T_V = 71.6°F$. To linearize the system, we used equation 6, which produces new dynamical equations, 7, 8 and 9.

$$f(x,u) \approx f(x^{eq},u^{eq}) + \sum_i^3 \frac{\partial f}{\partial x_i}(x^{eq},u^{eq}) * \left(x_i - x_i^{eq}\right) + \sum_i^3 \frac{\partial f}{\partial u_i}(x^{eq},u^{eq}) * \left(u_i - u_i^{eq}\right) \quad (6)$$

$$\begin{aligned} C_Z\dot{x}_1 = {} & \frac{1}{R_{AZ}}\left[u_1^{eq} - x_1^{eq}\right] + \frac{1}{R_{WZ}}\left[x_2^{eq} - x_1^{eq}\right] + \frac{1}{R_{FZ}}\left[x_3^{eq} - x_1^{eq}\right] + \rho c\, u_2^{eq}\left[u_3^{eq} - x_1^{eq}\right] \\ & - \left(\frac{1}{R_{AZ}} + \frac{1}{R_{WZ}} + \frac{1}{R_{FZ}} + \rho c\, u_2^{eq}\right) * \left(x_1 - x_1^{eq}\right) + \left(\frac{1}{R_{WZ}}\right) * \left(x_2 - x_2^{eq}\right) + \left(\frac{1}{R_{FZ}}\right) * \left(x_3 - x_3^{eq}\right) \\ & + \left(\frac{1}{R_{AZ}}\right) * \left(u_1 - u_1^{eq}\right) + \left(\rho c\left[u_3^{eq} - x_1^{eq}\right]\right) * \left(u_2 - u_2^{eq}\right) + \left(\rho c\, u_2^{eq}\right) * \left(u_3 - u_3^{eq}\right) \end{aligned} \quad (7)$$

$$C_W\dot{x}_2 = \frac{1}{R_{AW}}[u_1 - x_2] + \frac{1}{R_{WZ}}[x_1 - x_2] \quad (8)$$

$$C_F\dot{x}_3 = \frac{1}{R_{FZ}}[x_1 - x_3] \quad (9)$$

When we set up the dynamical equations into state space form, we see that almost all of the terms of equation 7 that do not contain a state or an input (i.e. the terms that are constant) disappear, with the exception of one term. Because u_2^{eq} = 0, this final term also disappears. Matrix A and B are seen below in equations 10 and 11.

$$A = \begin{bmatrix} -\frac{1}{C_Z}\left(\frac{1}{R_{AZ}} + \frac{1}{R_{WZ}} + \frac{1}{R_{FZ}} + \rho c\, u_2^{eq}\right) & \frac{1}{C_Z R_{WZ}} & \frac{1}{C_Z R_{FZ}} \\ \frac{1}{C_W R_{WZ}} & -\frac{1}{C_W}\left(\frac{1}{R_{AW}} + \frac{1}{R_{WZ}}\right) & 0 \\ \frac{1}{C_F R_{FZ}} & 0 & -\frac{1}{C_F R_{FZ}} \end{bmatrix} \quad (10)$$

$$B = \begin{bmatrix} \frac{1}{C_Z R_{AZ}} & \frac{1}{C_Z}\left(\rho c\left(u_3^{eq} - x_1^{eq}\right)\right) & \frac{1}{C_Z}\left(\rho c\, u_2^{eq}\right) \\ \frac{1}{C_W R_{AW}} & 0 & 0 \\ 0 & 0 & 0 \end{bmatrix} \quad (11)$$

Model Version 2
Controllable Inputs: $s(t)$
Uncontrollable Inputs: $T_A(t)$
Outputs: $T_z(t), T_w(t), T_f(t)$
Parameters: $R_{AZ}, R_{WZ}, R_{FZ}, R_{AW}, C_Z, C_W, C_F, P$

The following are the dynamical equations, state definition, and input definitions chosen for model 2. Model two is linear and does require any further linearization. In this model, the final term of the first dynamical equation is replace by the function s(t). This function is equal to 0 whenever the air flow rate falls below 400 cfm and equal to 1 whenever the air flow rate falls above 400 cfm.

$$C_Z\dot{T}_Z(t) = \frac{1}{R_{AZ}}[T_A(t) - T_Z(t)] + \frac{1}{R_{WZ}}[T_W(t) - T_Z(t)] + \frac{1}{R_{FZ}}[T_F(t) - T_Z(t)] + Ps(t) \quad (12)$$

$$C_W\dot{T}_W(t) = \frac{1}{R_{AW}}[T_A(t) - T_W(t)] + \frac{1}{R_{WZ}}[T_Z(t) - T_W(t)] \quad (13)$$

$$C_F\dot{T}_F(t) = \frac{1}{R_{FZ}}[T_Z(t) - T_F(t)] \quad (14)$$

$$\begin{bmatrix} x_1 \\ x_2 \\ x_3 \end{bmatrix} = \begin{bmatrix} T_z(t) \\ T_w(t) \\ T_f(t) \end{bmatrix} \quad (15)$$

$$\begin{bmatrix} u_1 \\ u_2 \end{bmatrix} = \begin{bmatrix} T_A(t) \\ s(t) \end{bmatrix} \quad (16)$$

Matrix A and B are seen below in equations 10 and 11.

$$A = \begin{bmatrix} -\frac{1}{C_Z}\left(\frac{1}{R_{AZ}} + \frac{1}{R_{WZ}} + \frac{1}{R_{FZ}}\right) & \frac{1}{C_Z R_{WZ}} & \frac{1}{C_Z R_{FZ}} \\ \frac{1}{C_W R_{WZ}} & -\frac{1}{C_W}\left(\frac{1}{R_{AW}} + \frac{1}{R_{WZ}}\right) & 0 \\ \frac{1}{C_F R_{FZ}} & 0 & -\frac{1}{C_F R_{FZ}} \end{bmatrix} \quad (17)$$

$$B = \begin{bmatrix} \frac{1}{C_Z R_{AZ}} & \frac{P}{C_Z} \\ \frac{1}{C_W R_{AW}} & 0 \\ 0 & 0 \end{bmatrix} \quad (18)$$

Parameter Identification

Although model versions 1 and 2 were both tested for parameter identification, model 2 produced more accurate results, so methodology for model 2 is shown below. The following are the dynamical equations expressed in theta-phi form.

$$\phi_1 = \begin{bmatrix} T_A(t) - T_Z(t) \\ T_W(t) - T_Z(t) \\ T_F(t) - T_Z(t) \\ s(t) \end{bmatrix} \quad (19)$$

$$\phi_2 = \begin{bmatrix} T_A(t) - T_W(t) \\ T_Z(t) - T_W(t) \end{bmatrix} \quad (20)$$

$$\phi_3 = [T_Z(t) - T_F(t)] \quad (21)$$

$$\theta_1 = \begin{bmatrix} \frac{1}{C_Z * R_{AZ}} & \frac{1}{C_Z * R_{WZ}} & \frac{1}{C_Z * R_{FZ}} & P \end{bmatrix} \quad (22)$$

$$\theta_2 = \begin{bmatrix} \frac{1}{C_W * R_{AW}} & \frac{1}{C_W * R_{WZ}} \end{bmatrix} \quad (23)$$

$$\theta_3 = \begin{bmatrix} \frac{1}{C_F * R_{FZ}} \end{bmatrix} \quad (24)$$

Once the dynamical equations were in theta-phi form, we loaded the training data and calculated the persistence of excitation. Our training data is from one classroom (room 110) in the LEEC that is using night flushing as its primary cooling method. Our full data set is from June 30th to October 16th. We used only the first ten days of data, June 30th to July 9th, as our training data. The following persistence of excitation results were produced: PE level for ϕ_1 is 0.0326, PE level for ϕ_2 is 1.1084, and PE level for ϕ_3 is 4.2929. All three PE levels are above zero, which indicates that the parameters are identifiable.

To identify the parameters, our first strategy was to use the gradient update law. We started by randomly choosing initial conditions for theta and a value for gamma, and then compared the final simulation to the training data. We iterated this process until we found initial conditions and a gamma that produced a simulation that was fairly representative of the training data. The best iteration was a result of the initial conditions and gamma seen in equations 25 through 28. These results can be seen in figures 2 through 5.

$$\theta_{1i} = [0.2 \quad 0.2 \quad 0.2 \quad 0.2] \tag{25}$$

$$\theta_{2i} = [0.2 \quad 1.0] \tag{26}$$

$$\theta_{1i} = [0.2] \tag{27}$$

$$\Gamma = 0.01 * I \tag{28}$$

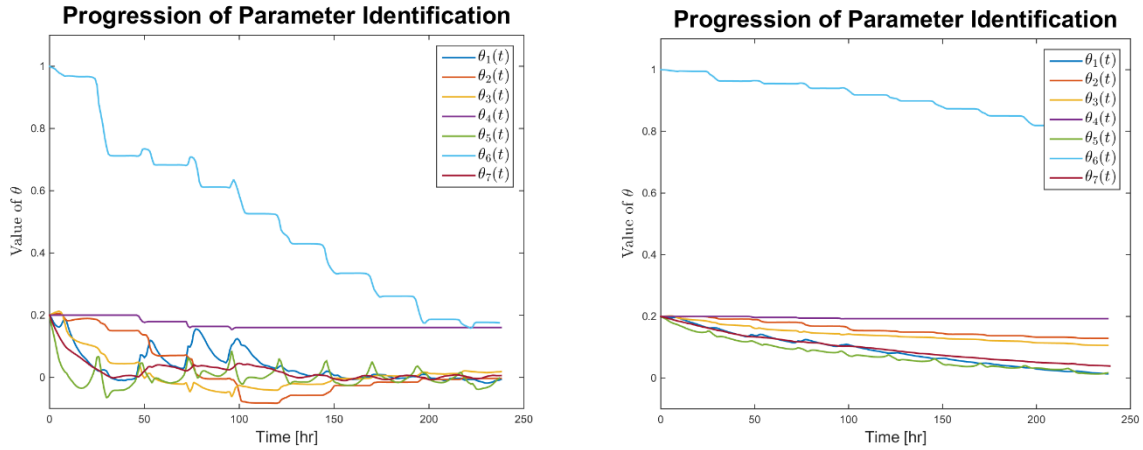

Figure 2: a) Progression of theta_hat over training data with gamma = 0.1, b) Progression of theta_hat over training data with gamma = 0.01

Parameter identification was unstable with a gamma of 0.1, as shown in figure 1a, by the spikes in theta_hat throughout the gradient update.

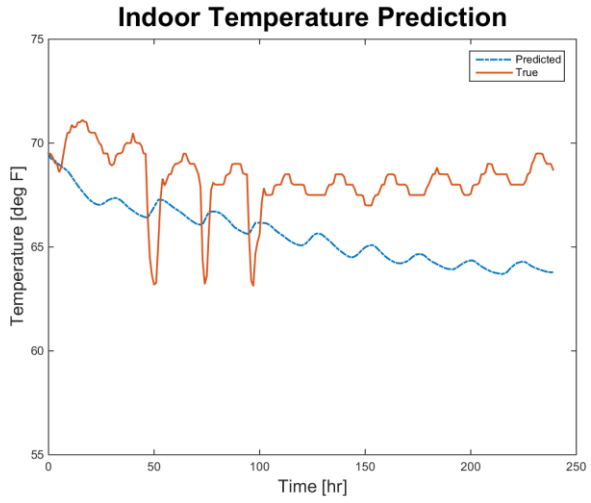

Figure 3: Predicted (from gradient descent) and true indoor air temperature over training data

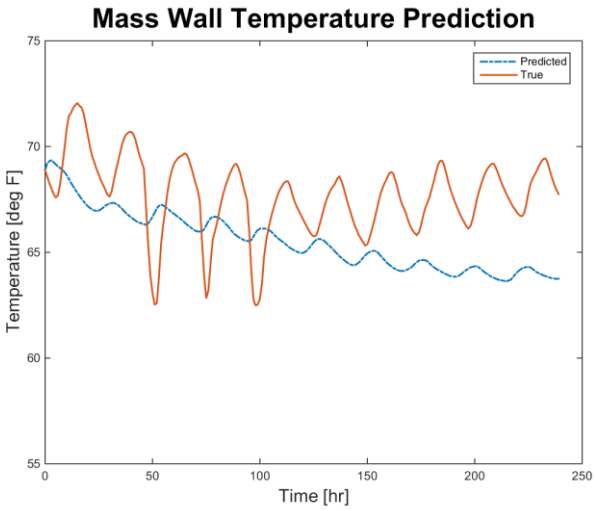

Figure 4: Predicted (from gradient descent) and true mass wall temperature over training data

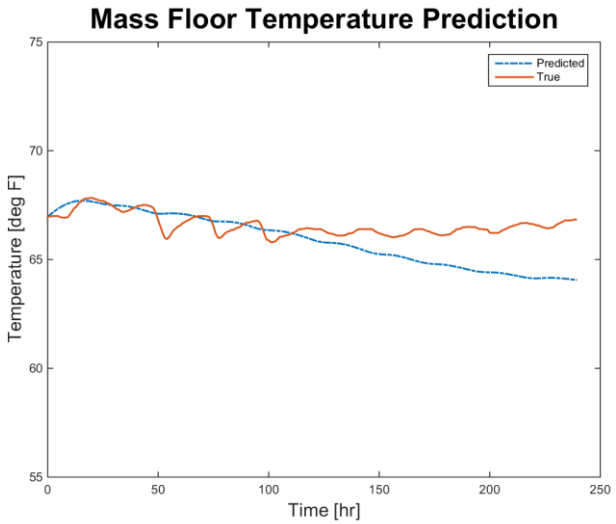

Figure 5: Predicted (from gradient descent) and true mass floor temperature over training data

Although these were the best results from the gradient descent, they were still not yet close enough to training data set to be a representative model. It was therefore decided to use an alternative estimation approach, known as the least square (LSQ) non-linear function. This method minimizes the square error between the simulation results and the training data. To begin the LSQ non-linear method, we input the final theta values from the gradient descent as initial estimates for theta. The function does 100 iterations for each parameter, so in this case 700 iterations. Once a set of 700 iterations was complete, we replaced the initial estimates for theta with the final values from the previous iteration. This process was done about 10 times until the simulations produced no further improvements in reducing the error. The results can be seen in figures 6 through 8 and the final values of theta can be seen in equations 29 to 31.

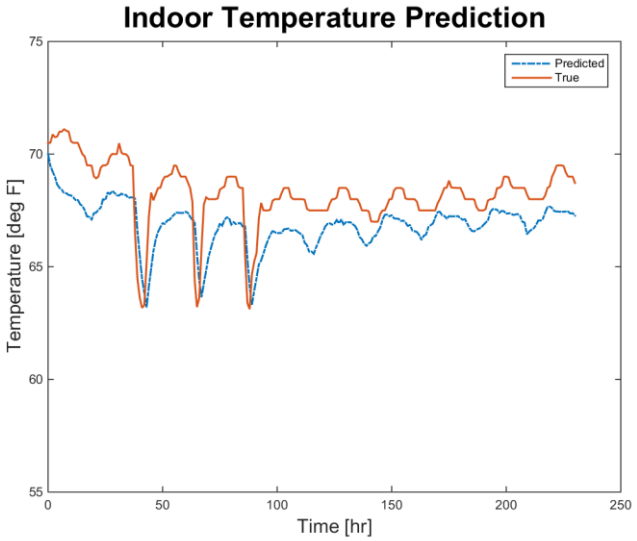

Figure 6: Predicted (from LSQ least-squares) and true indoor air temperature over training data

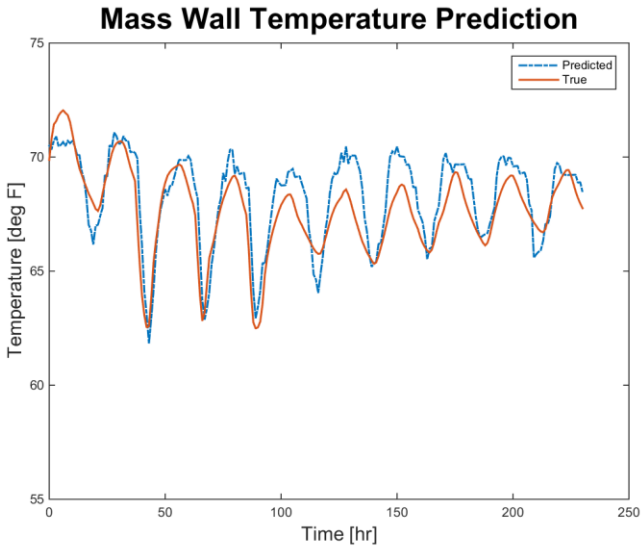

Figure 7: Predicted (from LSQ least-squares) and true mass wall temperature over training data

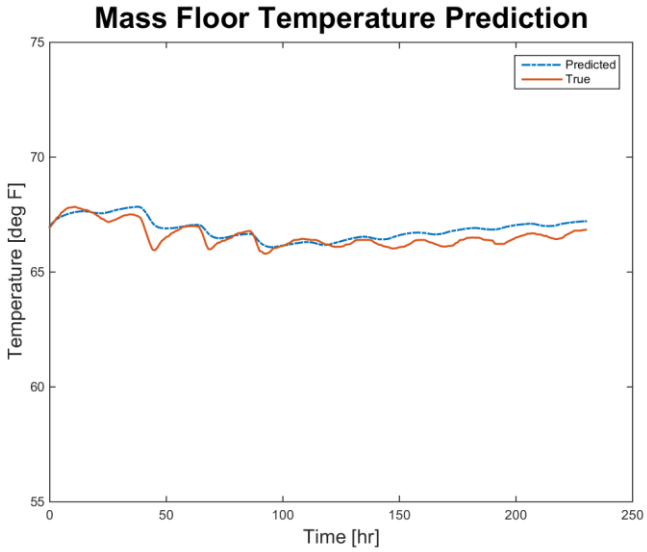

Figure 8: Predicted (from LSQ least-squares) and true mass floor temperature over training data

$$\hat{\theta}_1 = [-2.6356 \quad -11.0377 \quad 0.1790 \quad -0.9339] \tag{29}$$
$$\hat{\theta}_2 = [-8.7703 \quad 45.5929] \tag{30}$$
$$\hat{\theta}_3 = [0.0430] \tag{31}$$

It should be noted that the final parameters probably do not represent real physical characteristics because they were developed using a non-linear black box function.

Parameter Validation

Validation using Test Data

Our model was validated using two sets of test data, both from the same classroom as the training data, but from different dates. The first set of test data is from July 17th to July 25th. During this time span, the s(t) function remains constant at 0. The second set of test data is from September 4th to September 11th. During this time span, the s(t) function is both 0 and 1. The simulation results from both test data sets can be seen in the results section. It should be noted that our model produced better results for test data set 2.

Validation using Real Parameters

An alternative method to validate the model is to compare the model parameters to the "real" parameters. To find the real parameters, we first had to determine the physical properties of the room and room construction. To find these values, we used the mechanical and architectural construction documents. These properties can be seen in tables 2 and 3. Equations 32 through 39 show how each parameter was calculated.

Table 2: Description of room and material properties

Symbol	***Description***	***Units***		***Subscript***	***Description***
ρ	Density	[lb/ft^3]		Conc	Concrete
c	Specific Heat	[BTU/lb-°F]		Cem	Cement
t	Thickness	[in]		Ceil	Ceiling
L	Length	[ft]		Air	Air
W	Width	[ft]		room	Room
H	Height	[ft]		film, in	Inside air film
Rei	Thermal Resistance per Inch	[°F-ft^2-hr/(BTU-in)]		film, out	Outside air film
Re	Thermal Resistance	[°F-ft^2-hr/BTU]		ins	Insulation

Table 3: Values of room and material properties

Variable	***Value***
L_{room}	38
W_{room}	49.5
H_{room}	10
t_{conc}	4
t_{cem}	2
t_{ceil}	.5
ρ_{conc}	145
ρ_{cem}	95
ρ_{air}	0.0749
c_{conc}	0.23
c_{cem}	0.37
c_{air}	0.2403
Rei_{conc}	0.07
Rei_{cem}	0.26
Rei_{ceil}	0.45
Re_{ins}	20
$Re_{film,in}$	0.68
$Re_{film,out}$	0.17

$$R_{AZ} = \frac{Rei_{ceil} * t_{ceil} + Re_{film,in} + Re_{film,out}}{L_{room} * W_{room}} \quad (32)$$

$$R_{FZ} = \frac{Rei_{conc} * t_{conc}}{L_{room} * W_{room}} \quad (33)$$

$$R_{WZ} = \frac{(Rei_{cem} * t_{cem} + Re_{film,in})}{2 * (L_{room} + W_{room}) * H_{room}} \quad (34)$$

$$R_{AW} = \frac{(Re_{ins} + Re_{film,out})}{(L_{room} + W_{room}) * H_{room}} \quad (35)$$

$$C_Z = \rho_{air} * c_{air} * (L_{room} * W_{room} * H_{room}) \quad (36)$$

$$C_F = \rho_{conc} * c_{conc} * (L_{room} * W_{room} * \frac{t_{conc}}{12}) \quad (37)$$

$$C_W = \rho_{cem} * c_{cem} * (2 * (L_{room} + W_{room}) * H_{room} * \frac{t_{cem}}{12}) \quad (38)$$

The parameter of P represents the power of the ventilation system at maximum airflow. Therefore, we first had to determine what the maximum airflow was during our training data, and then find the time at which this airflow occurred. This time is designated as t^*.

$$P = \rho_{air} * c_{air} * V(t^*) * [T_a(t^*) - T_z(t^*)] \quad (39)$$

Finally, the "real" thetas can be seen in the results section. It should be noted that thetas from our model vary substantially from the thetas below. It should also be noted that simulations using the "real" thetas do not match the data, indicating that our dynamical equations may be too oversimplified to use real parameters in the model.

Optimization

The current setpoints in the actual building are causing the night flushing to overcool the room. Because the temperature of the room must fall within a specified comfort range during occupied hours, the system is doing a morning warmup before any occupants enter the building. This preheating is unnecessarily consuming energy that can be avoided through optimization. Figure 9 shows a sketch of the current control of the system in red.

You will see a new variable below for operative temperature (T_{OP}), which is a function of zone temperature, wall temperature, and floor temperature, as calculated in equation 40.

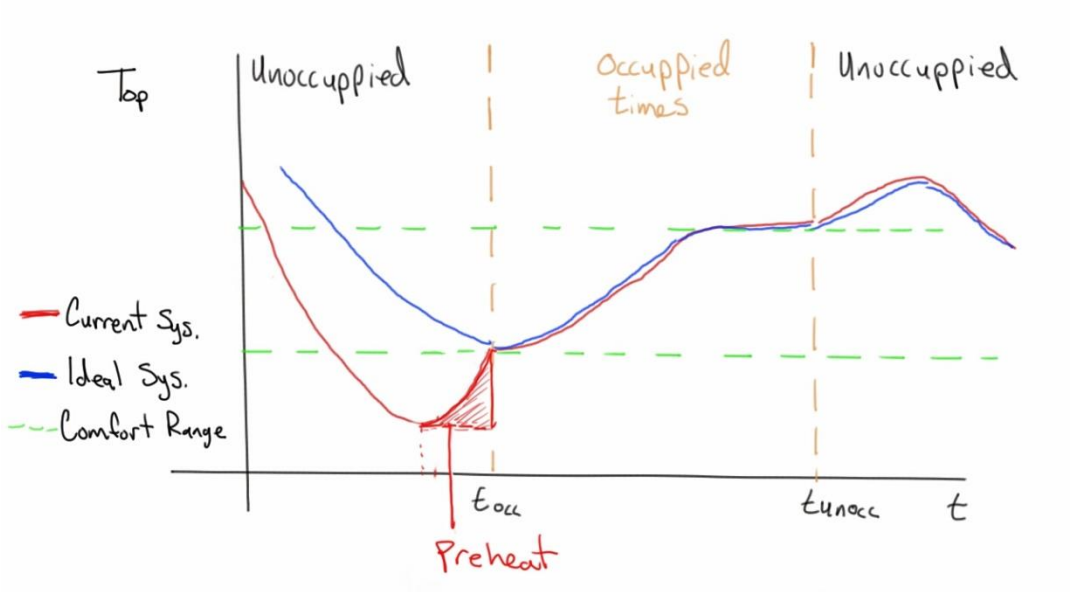

Figure 9: Operative temperature under current and ideal ventilation controls over a 24 hour period

$$T_{OP}(t) = \frac{1}{3}\left(T_Z(t) + T_W(t) + T_F(t)\right) \quad (40)$$

The objective function and constraints of our optimization try to fix this overcooling problem. Our objective is to reduce (or even eliminate) preheating, therefore we want the operative temperature to be very close to the minimum bound of the comfort range when occupancy begins. Because there are different temperature and ventilation requirements for occupancy, it is necessary to break down the constraints by occupied and unoccupied times. For our simulation, we are establishing the following occupancy schedule: occupied from 8AM-5PM and unoccupied from 5PM-8AM. Tables 4 and 5 show the optimization variables. Although our objective is to eliminate preheating, we are using the model that does not take supply temperature into account. Therefore, we had to come up with an objective function based only on the ventilation state variable. This translated to minimizing the cost associated with the ventilation system. Because it is assumed that the cost per unit energy is constant, the objective function is simply to minimize ventilation state at each time step. Equation 41 shows the objective function, and equations 42 through 49 show the equality and inequality constraints, which are based on the ASHRAE comfort zone.

Table 4: Description of optimization variables

Symbol	***Description***	***Units***		***Subscript***	***Description***
T	Temperature	[°F]		Occ	Occupied
s	Ventilation State	[0/1]		Unocc	Unoccupied
				Max	Maximum
				Min	Minimum
				OP	Operative

Table 5: Values of optimization variables

Variable	***Value***
$s_{Max,Occ}$	0
$s_{Max,Unocc}$	1
$s_{Min,Occ}$	0
$s_{Min,Unocc}$	0
$T_{OP,Max,Occ}$	78
$T_{OP,Max,Unocc}$	85
$T_{OP,Min,Occ}$	69
$T_{OP,Min,Unocc}$	60

$$\min_{s(t)}[s(t)] \tag{41}$$

$$s_{Occ} = s_{Max,Occ} \tag{42}$$

$$s_{Unocc} \leq s_{Max,Unocc} \tag{43}$$

$$s_{Occ} \geq s_{Min,Occ} \tag{44}$$

$$s_{Unocc} \geq s_{Min,Unocc} \tag{45}$$

$$T_{OP,Occ} \leq T_{OP,Max,Occ} \tag{46}$$

$$T_{OP,Unocc} \leq T_{OP,Max,Unocc} \tag{47}$$

$$T_{OP,Occ} \geq T_{OP,Min,Occ} \tag{48}$$

$$T_{OP,Unocc} \geq T_{OP,Min,Unocc} \tag{49}$$

As a first step, we decided to see where operative temperature falls in the training data set and both test data sets, based on the results of our model. These plots can be seen in the results section. While the model was doing a good job at predicting operative temperature, unfortunately it was not predicting temperatures above the minimum comfort criteria during occupied hours. Because the model was predicting operative temperature below the minimum comfort bound even with a continuous ventilation state of zero (see plot for test data set 1), we determined it would be nearly impossible to optimize this system. That being said, we laid out the methodology for optimization, if the model were to be offset and predict an operative temperature that falls within the comfort bounds or if the comfort bounds were to be adjusted downward.

To implement this optimization, we would use model predictive control. To begin this process, a simulation would be run over a period of 15 hours, from 5PM, the start of unoccupied hours, to 8AM, the end of unoccupied hours, with the ventilation state being equal to 0. We would then establish the boundary condition of the principle of optimality, seen in equation 50. Using dynamic programming, we would iterate backwards through each time step of the 15 hours to ensure that the operative temperature and ventilation state remained within their given bounds. Once the 15 hour period was optimized, we would move on to the next 15 hour period of unoccupied hours, using the final temperatures from the last occupied hour as initial conditions.

$$V_N = \begin{Bmatrix} 0 \middle| T_{op} = T_{OP,Min,Occ} \\ \infty \middle| T_{op} \neq T_{OP,Min,Occ} \end{Bmatrix} \tag{50}$$

Results

The follow 3 figures are simulation results from the parameter validation using test data.

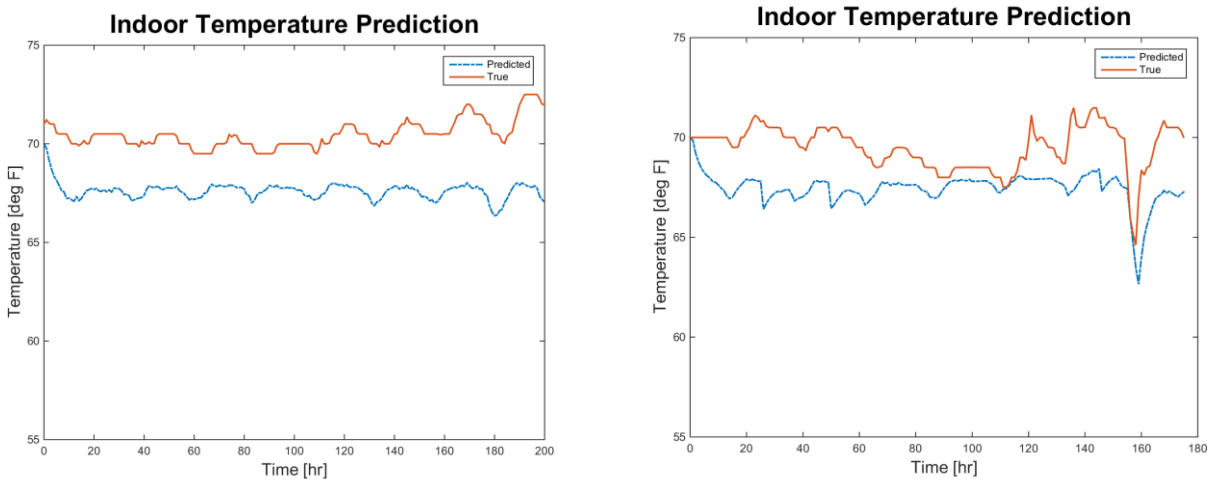

Figure 10: a) Predicted and true indoor air temperature over test data set 1, b) Predicted and true indoor air temperature over test data set 2

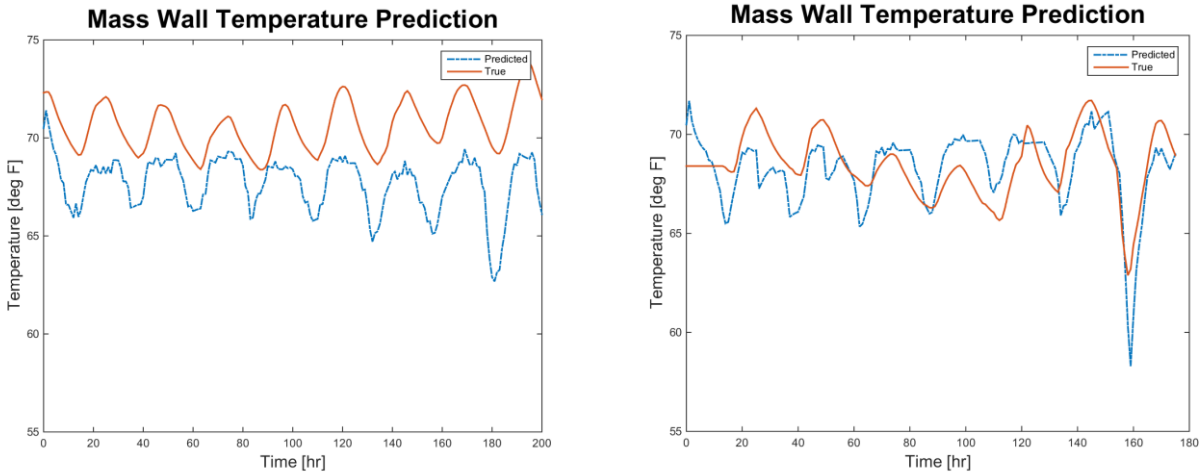

Figure 11: a) Predicted and true mass wall temperature over test data set 1, b) Predicted and true mass wall temperature over test data set 2

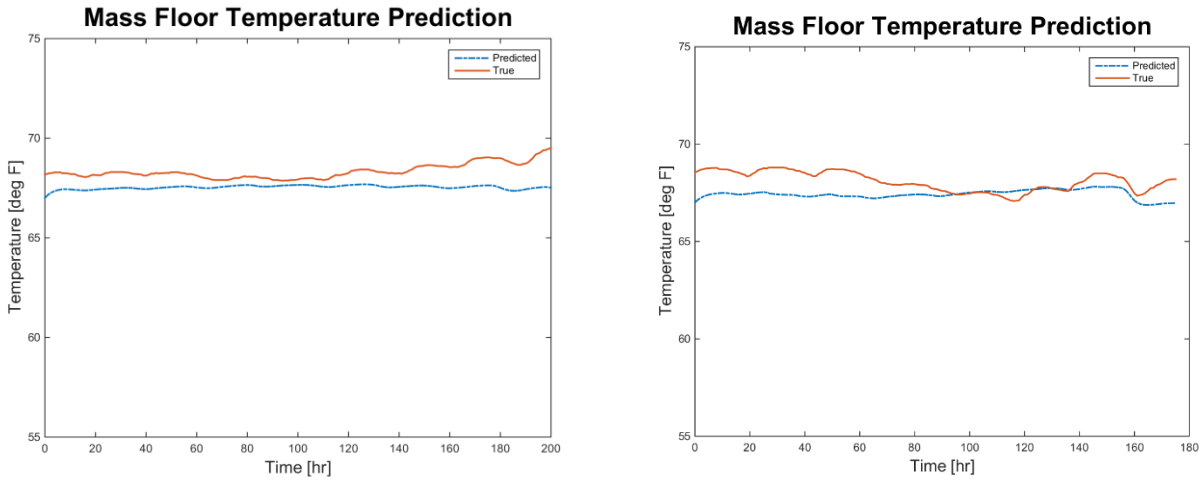

Figure 12: a) Predicted and true mass floor temperature over test data set 1, b) Predicted and true mass floor temperature over test data set 2

The following are the thetas from parameter validation using real room and material properties.

$$\theta_1 = [5.1661 \quad 4.3057 \quad 19.8342 \quad 2786.2955] \tag{51}$$
$$\theta_2 = [0.0042 \quad 0.1422] \tag{52}$$
$$\theta_3 = [0.3213] \tag{53}$$

The follow figures are simulation results of operative temperature from the training data and the two test data sets.

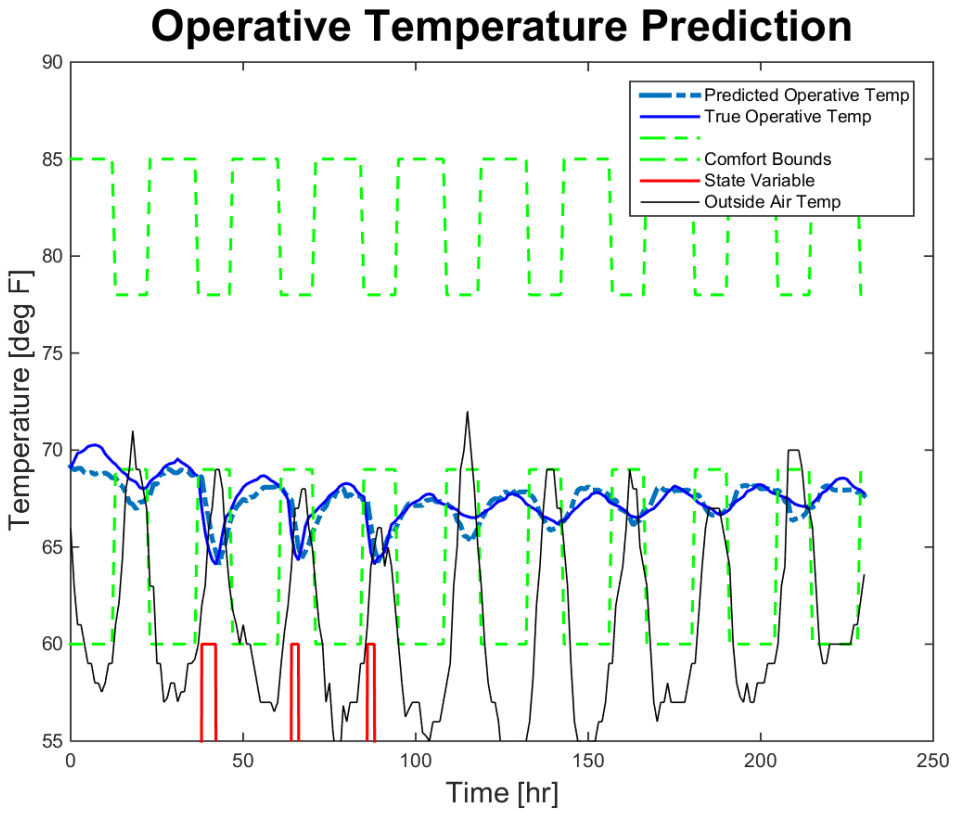

Figure 13: Outdoor air temperature and predicted and true operative temperature over training data set with comfort bounds

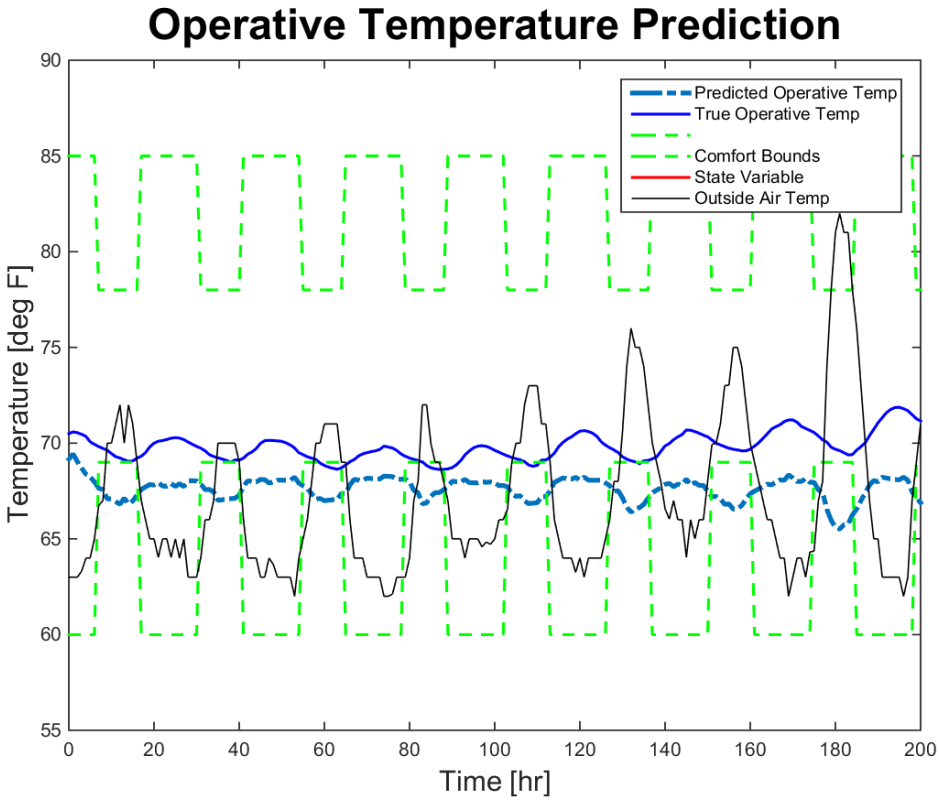

Figure 14: Outdoor air temperature and predicted and true operative temperature over test data set 1 with comfort bounds

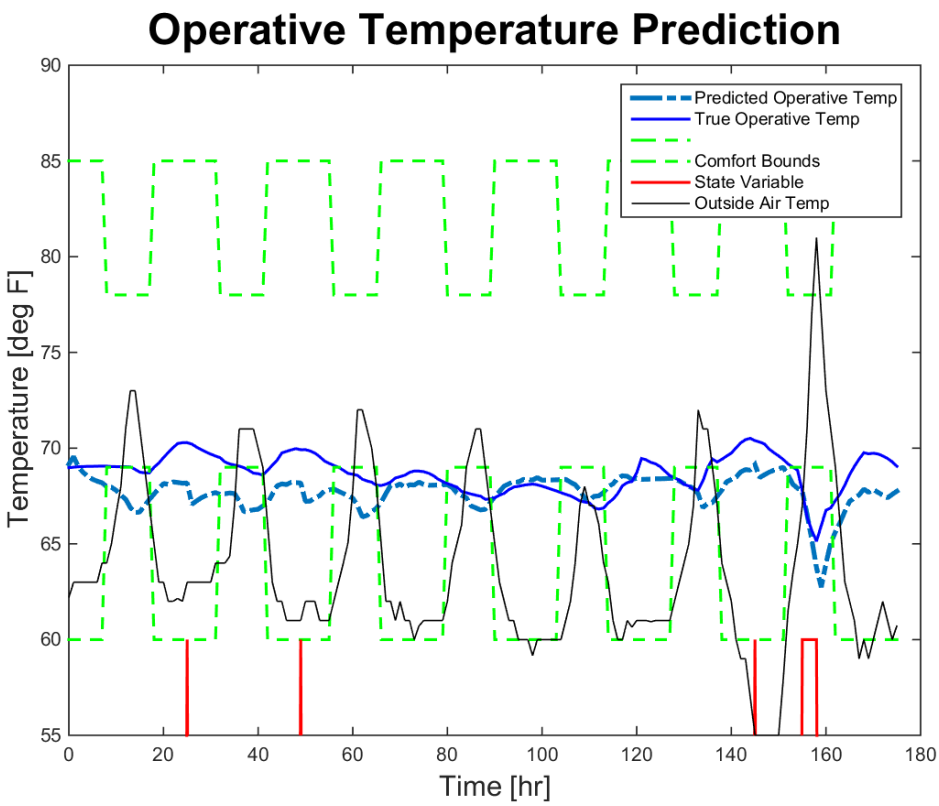

Figure 15: Outdoor air temperature and predicted and true operative temperature over test data set 2 with comfort bounds

Discussion

System Modeling

After conducting analysis for model version 1 and model version 2, we were first very surprised that version 1 performed worse, as version 2 contained less information in its inputs. One possible reason for model 2 better predicting the temperature is that it was already linear and did not require any linearization, which is in itself an estimation of the true dynamical equations. In addition to the two models discussed in the paper, we also tried a third model, which was identical to version 2, but the ventilation state variable was allowed to exist in 3 states: 0 if the air flow was below 200 cfm, 1 if the airflow was between 200 and 400 cfm, and 2 if the airflow was above 400 cfm. The second state represented normal code-required ventilation and the third state represented night flushing. Although this model performed better than version 2 after the gradient descent, the 3 state model diverged during the non-linear least squares method as soon as the data entered night ventilation mode.

Although we were able to find a fairly predictive model, our dynamical equations definitely are not perfect. The model does not take any of the following into account:

1. Heat transfer between the ground and the floor
2. Windows in the walls
3. A classroom on the second story between the ceiling and the outside air

In addition to these inaccuracies, the temperatures we used for the floor and walls were from sensors embedded within the mass, but the model really should have used surface temperatures. Unfortunately, there were no surface temperature sensors installed in the building. Finally, our equation for operative temperature was oversimplified and in reality, we would need to first calculate the mean radiant temperature. These discrepancies in our model might explain why the "real" parameters did not successfully predict temperature when implemented in the model.

Parameter Identification

In the end, we were able to identify parameters that fit our model fairly well. The errors between true and predicted data for indoor air temperature, mass wall temperature, mass floor temperature, and operative temperature are all small enough to consider our model to be a success. Both the gradient descent method and non-linear least squares method were essential in finding the final versions of our parameters. When we tried only using the gradient descent method, the parameters did not converge. If we increased the value of gamma to make the values converge, the model was unstable. While we were able to get a stable model with parameters that converged using the non-linear least squares method, this technique is unfortunately completely black-box. Therefore the values we got for our final parameters are definitely not representative of the real parameters. In other words, these parameters have no physical meaning, but they are simply numbers that fit our training data. This is yet another reason why the "real" parameters do not match the final parameters of our model.

Optimization

As previously mentioned, in almost all circumstances, the operative temperature during occupied hours falls below the lower bound of the comfort zone. Because this is true even when the ventilation state is continuously at 0, it is likely that the building might have an over cooling problem simply due to its construction, without even considering the ventilation system. For optimization purposes, we considered shifting the comfort zone down, forcing the operative temperature to fall within the comfort zone. However, based on results from the comfort tool developed by the Center for the Built Environment (CBE), as seen in figure 16, it is clear that the lower bound

for comfort is even higher than our original value of 69°F. Therefore, we could not justify lowering the comfort bound even further. Another method could be optimizing the system using version 1 of the model. This would allow for taking supply temperature into account. The cost function of this optimization would have to change to incorporate the cost of energy from heating. Because the room seems to be too cold even without ventilation, it is likely that energy would significantly increase from heating.

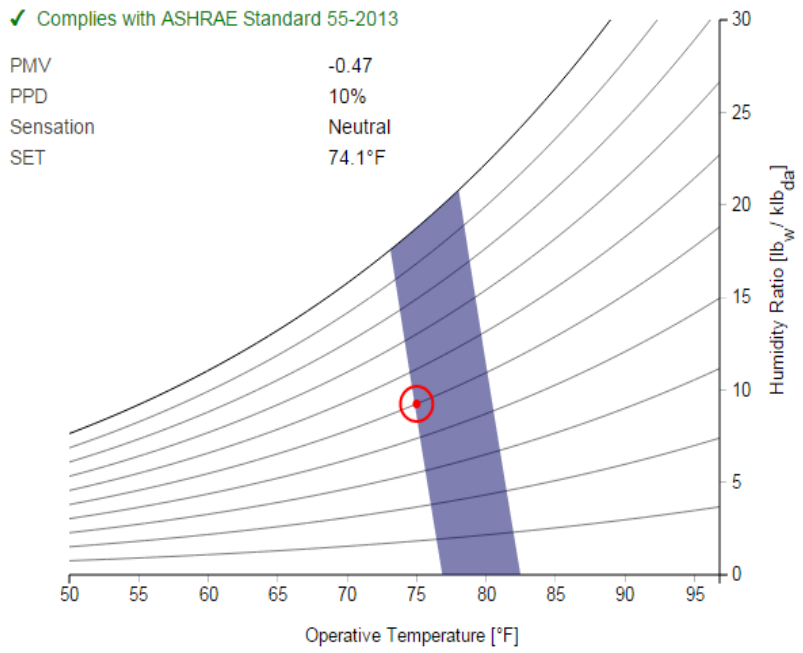

Figure 16: Comfort zone based on Center for the Built Environment comfort tool

Summary

The La Escuelita Education Center, in Oakland, CA, is using night flushing as its primary cooling method. Because it is typically difficult to forecast temperature when thermal mass is involved, we set an objective to create a model that predicts indoor air temperature and mass temperature. We developed two different models using dynamical equations, one with controllable inputs of supply temperature and ventilation rate, and the other with a controllable input of ventilation state. Using the model with ventilation state, we identified the parameters, first using the gradient descent method, and then using the non-linear least squares method. We then validated our model using test data and compared our final parameters to values calculated from real material and room properties. Finally, we laid out the methodology for optimization of the ventilation controls to eliminate overcooling, using model predictive control and dynamic programming.

References

[1] U.S. Energy Information Administration, “Commercial Building Energy Consumption Survey (CBECS),” 2012. [Online]. Available: http://www.eia.gov/tools/faqs/faq.cfm?id=86&t=1. [Accessed: 26-Feb-2015].

[2] S. Liu and G. P. Henze, “Experimental analysis of simulated reinforcement learning control for active and passive building thermal storage inventory: Part 1. Theoretical foundation,” *Energy Build.*, vol. 38, no. 2, pp. 142–147, Feb. 2006.

[3] J. Braun, “Reducing Energy Costs and Peak Electrical Demand Through Optimal Control of Building Thermal Storage,” *ASHRAE Trans.*, vol. 96, no. 2, pp. 876–887, 1990.

[4] J. E. Braun, “Load Control Using Building Thermal Mass,” *J. Sol. Energy Eng.*, vol. 125, no. 3, pp. 292–301, Aug. 2003.

[5] M. Kintner-Meyer and A. F. Emery, “Optimal control of an HVAC system using cold storage and building thermal capacitance,” *Energy Build.*, vol. 23, no. 1, pp. 19–31, Oct. 1995.

[6] G. P. Henze, C. Felsmann, and G. Knabe, “Evaluation of optimal control for active and passive building thermal storage,” *International Journal of Thermal Sciences*, vol. 43, no. 2, pp. 173–183, Feb. 2004.

[7] G. P. Henze, J. Pfafferott, S. Herkel, and C. Felsmann, “Impact of adaptive comfort criteria and heat waves on optimal building thermal mass control,” *Energy and Buildings*, vol. 39, no. 2, pp. 221–235, Feb. 2007.

[8] K. Lee and J. E. Braun, “Model-based demand-limiting control of building thermal mass,” *Building and Environment*, vol. 43, no. 10, pp. 1633–1646, Oct. 2008.